

Control of Microtubule Dynamics and Length by Cyclin A- and Cyclin B-dependent Kinases in *Xenopus* Egg Extracts

Fulvia Verde,* Marileen Dogterom,† Ernst Stelzer,* Eric Karsenti,* and Stanislas Leibler‡

*EMBL, Meyerhofstrasse 1, D-6900 Heidelberg, Germany; and †CEA, Service de Physique Théorique de Saclay, F-91191 Gif sur Yvette Cedex, France

Abstract. In eukaryotic cells, the onset of mitosis involves cyclin molecules which interact with proteins of the *cdc2* family to produce active kinases. In vertebrate cells, cyclin A dependent kinases become active in S- and pro-phases, whereas a cyclin B-dependent kinase is mostly active in metaphase. It has recently been shown that, when added to *Xenopus* egg extracts, bacterially produced A- and B-type cyclins associate predominantly with the same kinase catalytic subunit, namely p34^{cdc2}, and induce its histone H1 kinase activity with different kinetics. Here, we show that in the same cell free system, both the addition of cyclin A and cyclin B changes microtubule behavior. However, the cyclin A-dependent kinase does not induce a dramatic shortening of centrosome-nucleated microtubules whereas the cyclin B-dependent kinase does, as previously reported. Analysis of the parameters of microtubule dynamics by fluorescence video microscopy

shows that the dramatic shortening induced by the cyclin B-dependent kinase is correlated with a several fold increase in catastrophe frequency, an effect not observed with the cyclin A-dependent kinase. Using a simple mathematical model, we show how the length distributions of centrosome-nucleated microtubules relate to the four parameters that describe microtubule dynamics. These four parameters define a threshold between unlimited microtubule growth and the establishment of steady-state dynamics, which implies that well defined steady-state length distributions can be produced by regulating precisely the respective values of the dynamical parameters. Moreover, the dynamical model predicts that increasing catastrophe frequency is more efficient than decreasing the rescue frequency to reduce the average steady state length of microtubules. These theoretical results are quantitatively confirmed by the experimental data.

IN eukaryotes, progression through the cell division cycle requires the activity of kinases which control the structural and biochemical events specific of each cell cycle phase (Draetta and Beach, 1989; Minshull, 1989; Nurse, 1990). The catalytic subunits of these kinases are encoded by a family of *cdc2* related genes whereas regulatory subunits are encoded by a family of cyclin genes (Hunt, 1989; Hunter and Pines, 1991). It has been observed that, at least in the case of multicellular organisms, a kinase associated with cyclin A is activated during S-phase and remains active throughout prophase. Moreover, this kinase is inactivated during metaphase, while another kinase activity associated with cyclin B becomes important (Giordano et al., 1989; Minshull et al., 1990; Pines and Hunter, 1990). In agreement with the timing of its activation, cyclin A dependent kinase seems to be required at the G1-S and G2-M transitions (Pagano et al., 1992). Although its exact function is still unclear, it seems to regulate the nucleating activity of centrosomes (Buendia et al., 1992) and to play a role in DNA replication (Pagano et al., 1992). The cyclin B-depend-

ent kinase is probably involved in nuclear envelope breakdown (Heald and McKeon, 1990; Peter et al., 1990; Ward and Kirschner, 1990), inhibition of endosome fusion (Thomas et al., 1992; Tuomikoski et al., 1989) and mitotic spindle assembly (Murray and Kirschner, 1989). It is not clear, however, if the two kinases have entirely different functions, if they can substitute for each other or if they have only partially overlapping functions (Hutner and Pines, 1991; Minshull et al., 1990). It is therefore essential to establish detailed causal relationships between the activity of these cyclin-dependent kinases and the structural and dynamical changes that take place during different cell cycle phases. For instance, in the study of mitosis, one can ask whether the kinase activities associated with cyclin A and cyclin B have similar effects on the changes in microtubule dynamics associated with spindle assembly (Karsenti, 1991; McIntosh and Hering, 1991; Mitchison and Sawin, 1990; Salmon, 1989).

In this article, we address such questions by comparing the effects of cyclin A- and cyclin B-dependent kinases on the assembly of microtubules nucleated by centrosomes in frog egg extracts that closely mimic in vivo conditions (Lohka and Maller, 1985). We find that both kinases produce well-defined, but different, steady state length distributions of

Marileen Dogterom and Stanislas Leibler's present address is Princeton University, Physics Department, Jadwin Hall, P. O. Box 708, Princeton, NJ 08544.

the centrosome-nucleated microtubules. These structural changes in microtubule length distributions are correlated with specific changes in assembly dynamics. We present a mathematical analysis which shows how, through a modulation of the parameters of microtubule dynamics, the cyclin-dependent kinases can modify the length distributions of centrosome-nucleated microtubules. The results of the model agree quantitatively with the dynamic measurements made using video-enhanced fluorescence microscopy.

Materials and Methods

Materials

Human cyclin A produced in bacteria in a soluble form and purified according to Pagano et al., was obtained from G. Draetta (EMBL, Heidelberg, Germany) (Pagano et al., 1992). Purified sea urchin $\Delta 90$ cyclin B was obtained from M. Glotzer (Glotzer et al., 1991). Human centrosomes were prepared according to Bornens et al. (Bornens et al., 1987) from KE 37 lymphoblasts.

Frog Eggs

Xenopus females were injected with 100 U PMSG (Chronogest 500; Intervet, Holland) at least 3 d before use. Frogs were induced to lay eggs by injection of human chorionic gonadotropin (HCG¹; Sigma Chemical Co., St. Louis, MO) the night before. After injection with HCG, the frogs were kept in 1 liter of 0.1 M NaCl to avoid egg activation. The eggs were collected and rinsed several times in MMR/4 (1 \times MMR is 0.1 M NaCl, 2 mM KCl, 1 mM MgSO₄, 2 mM CaCl₂, 5 mM Hepes, 0.1 mM EDTA, pH 7.5) and the Jelly coat removed in 2% cysteine (pH 7.8).

Preparation of the Extracts

Interphase arrested extracts were prepared from electrically activated eggs, incubated in 100 μ g/ml cycloheximide for 90 min as previously described (Verde et al., 1990). The buffer used to prepare the extracts contained 100 mM K-Acetate, 2.5 mM Mg-Acetate, 60 mM EGTA, 10 μ g/cytochalasin D, 1 mM DTT (pH 7.2). Packed eggs were crushed by centrifugation at 10,000 g for 15 min in a minimum volume of buffer. An ATP regenerating system (1 mM ATP, 10 mM creatin phosphate, 80 μ g/ml creatin phosphokinase, final concentration) was added to the extract before further centrifugation at 100,000 g. The histone H1 kinase activity was measured as previously described (Félix et al., 1989) on histone H1 type IIIS (Sigma Chemical Co.).

Visualization of Microtubules by Immunofluorescence

Microtubule polymerization was studied as in (Verde et al., 1990) in 15- μ l aliquots of extracts incubated at room temperature in the presence of centrosomes (10³/ μ l of extract). Microtubules were visualized by immunofluorescence after fixation of the extracts by dilution in 1 ml of 0.25% glutaraldehyde in RG1 (80 mM Pipes, 1 mM EGTA, 1 mM MgCl₂, 1 mM GTP, pH 6.8 with KOH). After 6 min at room temperature, the suspension was layered on a 5-ml cushion of 25% glycerol (vol/vol) in RG2 (RG1 without GTP) in 15-ml corex tubes and centrifuged on a coverslip as described by Evans et al. (1985). The coverslips were postfixed in methanol at -20°C for 5 min and treated with freshly prepared 0.1% sodium borohydride (S-9125; Sigma Chemical Co.) in PBS for 10 min at room temperature. Immunofluorescence was performed with a polyclonal rabbit anti-tubulin and fluorescein-conjugated goat anti-rabbit antibody, diluted in PBS containing 3% BSA and 0.1% NaN₃. The coverslips were mounted in Moewiol, and photographs were taken using a Neofluar 100 \times lens, mounted on an Axiopt Photomicroscope (Carl Zeiss, Oberkochen, Germany), and recorded on TMY-400 films (Eastman Kodak Co., Rochester, NY).

Preparation of Fluorescent Tubulin

Calf brain tubulin was prepared by cycles of polymerization and depolymerization followed by phosphocellulose chromatography (Mitchison and Kirschner, 1984a,b) and labeled with tetramethylrhodamine succinimidyl

1. *Abbreviations used in this paper.* f_{cat} , catastrophe frequency; f_{res} , rescue frequency; g, growth; HCG, human chorionic gonadotropin; s, shrinking.

ester (Hyman et al., 1991). The stoichiometry of labeling was 1.24 mol of rhodamine per mol of tubulin and the concentration 34 mg/ml. The labeled tubulin was kept in liquid nitrogen in 2- μ l aliquots.

Video Microscopy

Centrosomes (10³/ μ l final concentration), rhodamine tubulin (3 μ M final) and an oxygen scavenging system (0.2 mg/ml catalase, 0.4 mg/ml glucose oxidase, 50 mM glucose, 4 mM DTT) were added to the extract after the pre-incubation with cyclins. Less than 1/10 of the volume of extract should be added for all components. 1.5 μ l of the mixture were squashed under a 24 \times 24 mm coverslip and sealed with Valap. The sample was observed for no longer than 30–40 min.

Recordings were performed using an Axiovert 10 (Carl Zeiss) microscope equipped with a standard Zeiss rhodamine filter set and a 63 \times (1.4 NA) Planapo Chromat objective. Images were collected through a Videoscope KS 1381 intensifier, processed with an image processor (Argus 10; Hamamatsu Phototronics, Hamamatsu City, Japan) and stored on a video-disc using a LV 6000 system (Sony, Montvale, NJ). To avoid photobleaching, the sample illumination was reduced using a Zeiss neutral density 4N filter and closing the aperture diaphragm in the epi-illumination tube to the minimum. Images were recorded every 5 s for the interphase and cyclin A-treated samples, and every 2 s for the cyclin B-treated samples. The shutter in front of the lamp was opened for 0.25 s, to collect and average eight frames (25 frames/s). Background subtraction, image averaging, shutter control, and recording were coordinated using homemade software available upon request.

Data Analysis

Microtubule asters recorded on the video disc were displayed on a video screen, frame by frame, and microtubule length measured with a cursor, using the functions available on the Hamamatsu Argus 10 image processor or an Image 1.5 program after frame grabbing in a MacIntosh II CI. For the measurements of the dynamic parameters only microtubules of which the plus end could be clearly seen over 0.5–2 min (typically 25 per experiment) were used. The center of each aster was determined visually and used as the origin of each microtubule measured in this aster. Growth (g) and shrinking (s) rates (v_g and v_s) were estimated by measuring changes in length over 15-s intervals for the interphase and cyclin A experiments and 10-s intervals for the cyclin B experiments (typical observed growth and shrinkage times were shorter for cyclin B-treated samples). The values are averages of these rates using typically 50 intervals for v_g and 25 for v_s . The catastrophe (rescue) events were determined by visual inspection of microtubule behavior as described in the curves shown in Fig. 3. Only clear and obvious transitions (see Fig. 3, arrows) were taken into account. Apparent poses or slight changes in rates were not considered as transitions, but treated as part of the growing and shrinking phases. The error we make in estimating the dynamical parameters this way is discussed in the "error evaluation and experimental limitations" section below. Catastrophe frequency (f_{cat}) and rescue frequency (f_{res}) were obtained by dividing the total number of recorded catastrophe (rescue) events by the total time spent in the growing (shrinking) phase over which the events were measured.

To determine microtubule average lengths in these experiments and compare them with values determined theoretically, only microtubules with lengths larger than $L_{min} = 5 \mu$ m (cyclin A) or 3 μ m (cyclin B) and smaller than $L_{max} = 20 \mu$ m were considered. L_{min} is set by the area around the centrosome in which it is impossible to see individual microtubules. It is larger in cyclin A than in cyclin B treated extracts because centrosomes nucleate more microtubules in the former case. The value of L_{max} is imposed by the video setup (field of view). Microtubule lengths were estimated in every fifth video frame using the same asters as those used for determining the values v_g , v_s , f_{cat} , and f_{res} .

Errors Evaluation and Experimental Limitations

There are several errors associated with the determination of the dynamical parameters v_g , v_s , f_{cat} , and f_{res} , as well as with the determination of microtubule average lengths on video frames. The optical resolution of our experimental setup, which determines how precisely we can locate visually the microtubule ends, varies between 0.2 and 0.5 μ m. Provided that the centrosome (and thus our reference point) does not move between one recorded frame and the next (a 2- or 5-s interval), a given microtubule has to grow or shrink at least 0.5 μ m in order for us to decide that it actually grew or shrank. It is this criterion that we used in deciding at what instants transitions between growing and shrinking phases occurred. The given errors as-

sociated with the values for f_{cat} and f_{res} are statistical errors due to the finite number of observed catastrophe (rescue) events. They are relatively large because in general few events were observed. For very few events (<7) only an upper bound for the actual rate could be estimated (the value between brackets for the rescue rates in the cyclin treated extracts) (Particle Data Group, 1990).

To estimate the average values for v_g and v_s we measured systematically length changes over fixed time intervals. We chose intervals of 15 s for interphasic- and cyclin A-treated extracts and 10 s for cyclin B-treated extracts (which is of the order of the shortest observed growth and shrinkage times) and checked that the exact choice of these intervals does not significantly affect the results. We use the velocity distribution that we find this way for every experiment to calculate the average growth or shrinkage rate. The error given in Table I represents the statistical error associated with this average value, due to the limited number of measurements and the dispersion that we find. Note that when we estimate the length difference between microtubules that are separated in time by several frames, an additional error shows up because we have to choose a new position for the center of the aster. Centrosomes sometimes move and we can not always keep our reference point in the center of the aster fixed. This error and the uncertainty in the location of the tip (we estimate that the total systematic error in one absolute length measurement can be around 1 μm) as well as real fluctuations in growth and shrinkage rates give rise to the observed dispersion in the velocity distributions.

The error given for the average length measurements represents again a statistical error, due to the limited number of measurements and the variability between the analyzed frames. Because we measure several hundreds of microtubules per experiment, this error is much smaller than the systematic error for one individual length measurement, which, as stated above, we estimate to be $\sim 1 \mu\text{m}$. One should note that in order to compare theoretically obtained average lengths with the measured average values one has to take into account the geometry of the experimental set up (see following section and Fig. 6).

In the following we discuss some experimental limitations that we think should be kept in mind: for the measurements of the average microtubule steady state lengths, our definition of absolute microtubule length (the distance between the center of the aster and the tip of the microtubule) is not entirely realistic. We do not know where in the centrosome the microtubules exactly start to grow. However, this fact is not very relevant for our results

because we are forced (by the size of the bright region in the center) to study length distributions relatively far from the centrosome. These distributions are not affected by the exact location at which microtubules are nucleated.

To estimate the dynamical parameters, we follow microtubules that grow inside the focal field for a certain time. The finite depth of the focal field (1–2 μm) allows them to grow under a small angle with respect to the focal plane, which leads to an underestimation of the measured growth and shrinkage rates of ~ 1 –3%. We neglected this effect.

Apart from statistical errors the measurements of the dynamical parameters, in particular those of the transition frequencies, are subject to important systematic errors due to the finite spatial and temporal resolution of the microscope. For instance, if a “catastrophe” and a following “rescue” event occurring on a given microtubule are separated by a time interval shorter than the period between two video frames, or if the microtubule shrinks during this time by a distance shorter than the optical length resolution (0.5 μm here), one misses these events. This may result in transitions that do not seem always abrupt and render the interpretation of apparent “pauses” and changes in instantaneous growth or shrinking rates difficult because pauses and changes in assembly rates do seem to exist independently of these effects (Cassimeris et al., 1988; Schulze and Kirschner, 1988; Gildersleeve et al., 1992). To estimate the importance of the fact that we filter out some events, we performed a numerical simulation of dynamical microtubules, characterized by four dynamical parameters, and then “measured” these parameters with the resolution of the experiments. We could then adjust the theoretical parameters so that the “measured” values match the ones observed in the experiment. We find that the theoretical values we had to choose for the velocities v_g and v_s are ~ 2 –5% larger than the measured values, while for f_{cat} and f_{res} these theoretical values had to be ~ 10 –30% larger than the experimentally observed values. These differences are usually smaller than, or in the range of, the statistical errors due to limited number of measurements.

In addition to systematic and statistical errors due to the finite spatial and temporal resolution of the microscope, the measured values of the dynamical parameters and steady state lengths may be influenced by interferences between growing asters, interactions with the coverslips, local inhomogeneities or aging of the proteins. As previously discussed (Belmont et al., 1990), special care has to be taken to avoid the presence of oxygen in the extracts, illumination must be kept as low as possible and the rhodamine-tubulin concentration should be a small fraction (1/5th–1/10th)

Table I. The Parameters of Microtubule Dynamics in *Xenopus* Egg Extracts

	v_g	v_s	f_{cat}	f_{res}	J	$\langle L \rangle$
	($\mu\text{m}/\text{min}$)	($\mu\text{m}/\text{min}$)	(1/s)	(1/s)	($\mu\text{m}/\text{min}$)	(μm)
Interphase	6.5 ± 0.3	9.3 ± 0.5	0.012 ± 0.003	0.020 ± 0.005	+0.58	
	7.6 ± 0.4	9.4 ± 0.5	0.011 ± 0.003	0.016 ± 0.005	+0.67	
Cyclin A						
25 nM	9.8 ± 0.6	9 ± 1	0.011 ± 0.004	$0.010 (<0.016)$	– 0.05	
50 nM	8.9 ± 0.4	16 ± 2	0.013 ± 0.004	$0.004 (<0.010)$	–10.1	14 ± 7
100 nM	11.1 ± 0.7	10.6 ± 0.9	0.018 ± 0.005	$0.004 (<0.010)$	– 6.7	13 ± 7
	9.7 ± 0.4	12.3 ± 0.7	0.025 ± 0.004	$0.005 (<0.011)$	– 8.6	8 ± 2
	10.6 ± 0.4	13.6 ± 0.9	0.016 ± 0.004	$0.007 (<0.011)$	– 6.2	17 ± 7
Cyclin B						
500 nM	8.8 ± 0.7	13.7 ± 0.9	0.05 ± 0.01	$0.006 (<0.010)$	–11.3	3.2 ± 0.8
	8.3 ± 0.5	10.6 ± 0.9	0.06 ± 0.01	$0.003 (<0.007)$	– 9.5	2.9 ± 0.7

Average polymerization (v_g), depolymerization (v_s), catastrophe (f_{cat}), and rescue (f_{res}) rates for microtubules in interphase, cyclin A-, and cyclin B-treated extracts, together with the corresponding calculated values of J (average microtubule growth rate) and $\langle L \rangle$ (average microtubule steady state length). Experiments were conducted in the same extract (stored frozen in liquid nitrogen). Rhodamine tubulin was added at a concentration of 0.3 mg/ml and the endogenous tubulin concentration was about 15 μM as evaluated by immunoblotting (Similar results were obtained in different extracts). Microtubules of which the end could be clearly seen over 0.5–2 min (typically 25 per experiment) were used. Polymerization and depolymerization rates were estimated by measuring changes in length over 15-s intervals for the interphase and cyclin A experiments and 10 sec intervals for the cyclin B experiments. The values are averages of these rates associated with the expected error over the total number of intervals per experiment (typically 50 for polymerization rates and 25 for depolymerization rates). The catastrophe (rescue) events were estimated by dividing the total number of observed catastrophe (rescue) events by the total time spent in the growing (shrinking) phase over which the events were measured. The given standard errors are relatively large because in general few events were observed. For very few events (less than seven) only an upper bound for the actual rate could be estimated (the value between brackets for the rescue rates in the cyclin treated extracts) (Particle Data Group, 1990). The values of J and $\langle L \rangle$ were calculated from the dynamical parameters with equations 5 and 8. Standard error propagation (Particle Data Group, 1990) provides the error in $\langle L \rangle$. Note that, because of the non-linear dependence on the transition rates (f_{cat} , f_{res}) and the large uncertainties for these rates, this error turns out to be especially large for large values of $\langle L \rangle$. The histone H1 kinase produced by cyclin A was 4–5, 8–10, and 15–25 pmol/min/ μl of extract at 25, 50, 100 nM, respectively, and that produced by cyclin B was 15–20 pmol/min/ μl at 500 nM.

of the whole tubulin concentration present in the extract. We remained in these limits and we reproduced the results of Belmont et al. (1990) concerning the shortening effect of rhodamine-tubulin on centrosome-nucleated microtubules visualized by centrifugation and immunofluorescence on coverslips. With the ratio of rhodamine-tubulin/cold tubulin in our experiments, the shortening effect should be around 20% (Belmont et al., 1990). We used the same concentration of rhodamine-tubulin in all experiments. To compare the effect of light irradiation on microtubule dynamics, in one experiment the same cyclin A-treated sample was recorded (and therefore illuminated) every 5 and every 2 s. We did not detect any difference in the parameters of microtubule dynamics.

Geometrical Correction

The theoretical steady state microtubule distributions were obtained assuming an exponential length distribution (equation 7), $\langle L \rangle$ being calculated using the dynamical parameters from the experimental recordings (equation 8). To compare the theoretical distributions with the experimentally observed length distributions and average lengths, the calculated exponential distributions were corrected to take into account the geometry of the experimental setup. On the video recordings, one does not measure the real lengths of the microtubules, but rather the projections onto the focal plane of the parts of microtubules which are in focus (i.e., inside the depth of field, shown schematically in the inset to Fig. 6). Each time we numerically simulated a three dimensional aster with an exponential length distribution where we supposed a random, isotropic distribution of microtubule orientations. Given the calculated average length $\langle L \rangle$ of this three dimensional distribution, we then estimated what should be their apparent length distribution in two dimensions for different values of the depth of field and different positions of the centrosome. This correction is important but not very sensitive to the exact value of the depth of field, d (Haferkorn, 1981) nor to the exact position of the centrosome within this area. The apparent average length of these distributions was, as in the experiments, calculated with a lower cut-off at L_{\min} and an upper cut-off at L_{\max} (see data analysis).

Results

Cyclin A- and Cyclin B-dependent Kinases Produce Microtubule Asters with Different Steady State Length Distributions

Concentrated *Xenopus* egg extracts are commonly used to study the dynamics of cellular organelle morphogenesis in interphase and mitotic environment in vitro (Belmont et al., 1990; Blow and Laskey, 1986; Dabauvalle et al., 1991; Hutchison et al., 1989; Lohka and Maller, 1988; Newport, 1987; Newport and Spann, 1987; Verde et al., 1990). In this work, we used extracts prepared from eggs arrested in interphase by inhibition of protein synthesis for 90 min during the first *Xenopus* embryonic cell cycle (Félix et al., 1990). These extracts were devoid of endogenous A and B type cyclins as revealed by immunoblot analysis with antibodies raised against the *Xenopus* molecules (not shown). The addition of human cyclin A (Pagano et al., 1992) or sea urchin $\Delta 90$ cyclin B (Glotzer et al., 1991) purified from transformed bacteria to these extracts resulted in a strong increase in the level of H1 kinase activity (Buendia et al., 1991). This is due to the association of the added cyclins with cdc2 molecules present in large excess in the egg extracts (Kobayashi et al., 1991). It has been shown that >80% of the H1 kinase activity produced by each cyclin can be attributed to the activation of p34^{cdc2} proper (Clarke et al., 1992). We first examined qualitatively the effects of cyclin A- and cyclin B-dependent kinases on centrosome-nucleated microtubules by fixing the extracts and staining the microtubules by immunofluorescence after centrifugation on glass coverslips (Verde et al., 1990). In interphase extracts, extensive spontaneous polymer assembly was observed and the centrosomes nucleated

very long microtubules (Fig. 1 a). The only factors limiting the growth of centrosome-nucleated microtubules seemed to be the decrease in free tubulin concentration due to the extensive spontaneous assembly and the finite size of the container. Addition of cyclin B to these extracts eliminated spontaneous polymer assembly and induced the formation of very short microtubule asters around the centrosomes (Fig. 1 b). This effect was similar to that of purified cdc2 kinase (Verde et al., 1990) and to findings of Belmont et al. (Belmont et al., 1990) who used the same cyclin B. Cyclin A also suppressed spontaneous polymer assembly in the extracts, but the centrosome-nucleated microtubules remained much longer than in the cyclin B-treated extracts (Fig. 1 c). A dose-response curve of microtubule length as a function of cyclin A or cyclin B concentration showed that adding 300 nM cyclin A or 500 nM cyclin B to interphase extracts produced an histone H1 kinase activity of 40-50 pmol/min/ μ l and 30 pmol/min/ μ l, respectively. Yet, in the cyclin A-treated extract, the longest microtubules remained about three times as large as in the cyclin B treated extract (Fig. 1), although at these cyclin concentrations 90% of the p34cdc2 molecules present in the extract were bound to the cyclins and activated (Clarke et al., 1992). We did not evaluate microtubule average lengths in these experiments because we could not measure the dynamic parameters directly and because they cannot be compared with the video-microscopy data given the fact that there is no rhodamine-labeled tubulin added to these extracts (see methods). In any case, it is clear that qualitatively, both in cyclin A- and in cyclin B-treated extracts, microtubules reach well defined but different steady state length distributions. This could not be attributed to a depletion of tubulin subunits because there is no spontaneous polymerization and the amount of tubulin incorporated into the asters is negligible compared to the total amount of tubulin present in the extracts (Verde et al., 1990). Nor could this be attributed to the finite size of the container, since the latter was much larger than the maximum length of the microtubules. One is thus left with the possibility that different steady state length distributions of the asters are produced in response to a specific regulation of the parameters of microtubule dynamics by cyclin A- and cyclin B-dependent kinases, for instance through a targeting towards specific substrates.

Cyclin A- and Cyclin B-dependent Kinases Affect Differently the Parameters of Microtubule Dynamics

The dynamical process underlying the assembly of microtubules is called "dynamic instability" (Mitchison and Kirschner, 1984a,b). In the simplest description of this phenomenon, a microtubule can polymerize with a linear velocity v_g or depolymerize with velocity v_s . These two states of growth and shrinkage are separated by apparently stochastic transition events called "catastrophes" (transitions growth \rightarrow shrinkage, with frequency f_{cat}) and "rescues" (transitions shrinkage \rightarrow growth, with frequency f_{res}). The four parameters v_s , v_g , f_{cat} , and f_{res} therefore characterize the dynamical properties of a population of microtubules (Carlier, 1991; Walker et al., 1988). To study this dynamical process we analyzed the behavior of centrosome-nucleated microtubules in egg extracts by video-enhanced fluorescence microscopy. Images on which microtubule dynamics was analyzed in interphase, cyclin B- and cyclin A-treated extracts

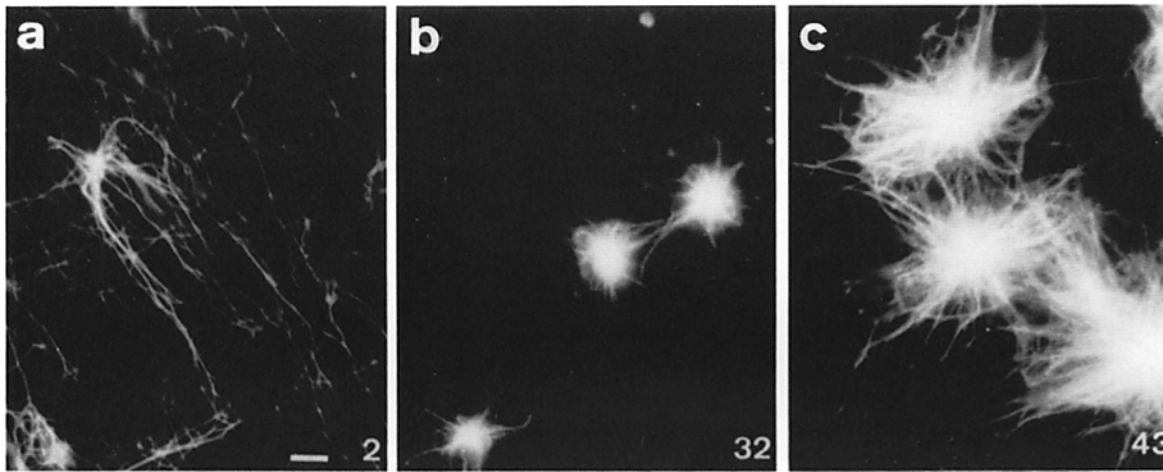


Figure 1. Effect of addition of cyclin A or B to interphase extracts on microtubule assembly. Cycloheximide-treated extracts were incubated with human centrosomes at room temperature for 15 min after pre-incubation for 45 min at room temperature in the absence (a) or in the presence of cyclin B (500 nM) (b) or cyclin A (300 nM) (c). The extract was then fixed and immunofluorescence performed as described in Materials and Methods. The histone kinase activity measured during the incubation is shown in the lower left corner. Bar, 5 μ m.

are shown in Fig. 2. The arrowheads point to examples of growing and shrinking microtubules. Again, we observed that cyclin B produced much shorter microtubule asters than cyclin A for the same level of kinase activity measured on histone H1, while both eliminated the free polymerization (Fig. 2). In interphase extracts microtubules remained anchored to the centrosomes. However, in the presence of both cyclin A- and cyclin B-dependent kinases, microtubules sometimes detached from the centrosomes and wandered away. This effect might be due to the activation of the mitotic microtubule severing activity (Vale, 1991). This is visible in the cyclin A-treated extract in Figure 2c. We did not take into account these free microtubules in our quantitative measurements. Examples of the dynamics of individual microtubules are shown in Fig. 3. The growing and shrinking periods as well as the transitions between them are clearly seen on these curves. The values of the parameters of microtubule dynamics in the different extracts, are shown in Table I. Keeping in mind the experimental limitations (see Methods), we can summarize the results presented in Table I as follows: (a) both cyclin A- and cyclin B-dependent kinases increase the velocities v_g and v_s , although this effect is relatively small (20–30%); (b) both cyclin dependent kinases seem to decrease the “rescue” frequency f_{res} . Because of the very small number of recorded events, the exact value of this parameter in cyclin-treated extracts was not well established, and therefore we give only an upper bound to the rescue frequencies; and (c) while cyclin B-dependent kinase increases several fold the “catastrophe” frequency f_{cat} , this is not the case for cyclin A-dependent kinase whose effect on f_{cat} hardly exceeds the resolution limits of the experiments. We routinely used cyclin B at 500 nM to ensure proper activation of the kinase (to a level of 15–20 pmol/min/ μ l) because cdc2 kinase is only activated when cyclin B concentration exceeds a threshold (50–100 nM), whereas this is not the case for cyclin A (Clarke et al., 1992). The range of cyclin A concentrations shown in Table I (from 25 to 100 nM), produced histone H1 kinase activities comprised between 5 and 20 pmol/min/ μ l of extract, which are close to or slightly above the physiological level of activity found in eggs. In these ex-

tracts, the maximum level of H1 kinase was obtained for 300 nM cyclin A (40–50 pmol/min/ μ l) and 1 μ M cyclin B (30 pmol/min/ μ l). These activities are way above the physiological levels. Yet, the cyclin A-dependent kinase did not shrink microtubules even when used at 300 nM. Therefore, the weak effect of cyclin A compared to cyclin B on f_{cat} is not due to a lower level of activation of the kinase. It is also unlikely to be due to an artefactual lack of function of the cyclin A used in these experiments since the same molecule affected other parameters of microtubule dynamics very similarly to the cyclin B. The cyclin A also increased the ejection rate of microtubules from the centrosomes (Belmont et al., 1990) and activated the microtubule severing activity (Vale, 1991) just as the cyclin B did (see Discussion).

Tying Together Microtubule Steady State Length Distributions and Dynamics within a Simple Model

In the previous sections, we have shown that cyclin A- and cyclin B-dependent kinases have different effects on the steady state length of centrosome-nucleated microtubules in egg extracts and on the parameters of microtubule dynamics. In the following, we examine a possible correlation between these effects by applying a theoretical model of microtubule dynamics to experimental data. We limited the analysis to a simple model of stiff, noninteracting polymers, growing in an infinite homogeneous medium. A similar model was previously studied by T. Hill (1987). In such a model, the transitions between the growing and shrinking phases are random events appearing with frequencies f_{cat} and f_{res} , and the addition and removal of subunits at microtubule plus ends are supposed to be stochastic processes with constant rates (corresponding to constant velocities v_g and v_s) (see Fig. 4). The microtubules are nucleated at the centrosome at a constant rate $\nu > 0$. Although each of these parameters may depend upon tubulin concentration, the presence of different stabilizing and destabilizing molecules or other biochemical parameters, this model makes use only of the effective values of v_g , v_s , f_{cat} , and f_{res} and does not require any assumption

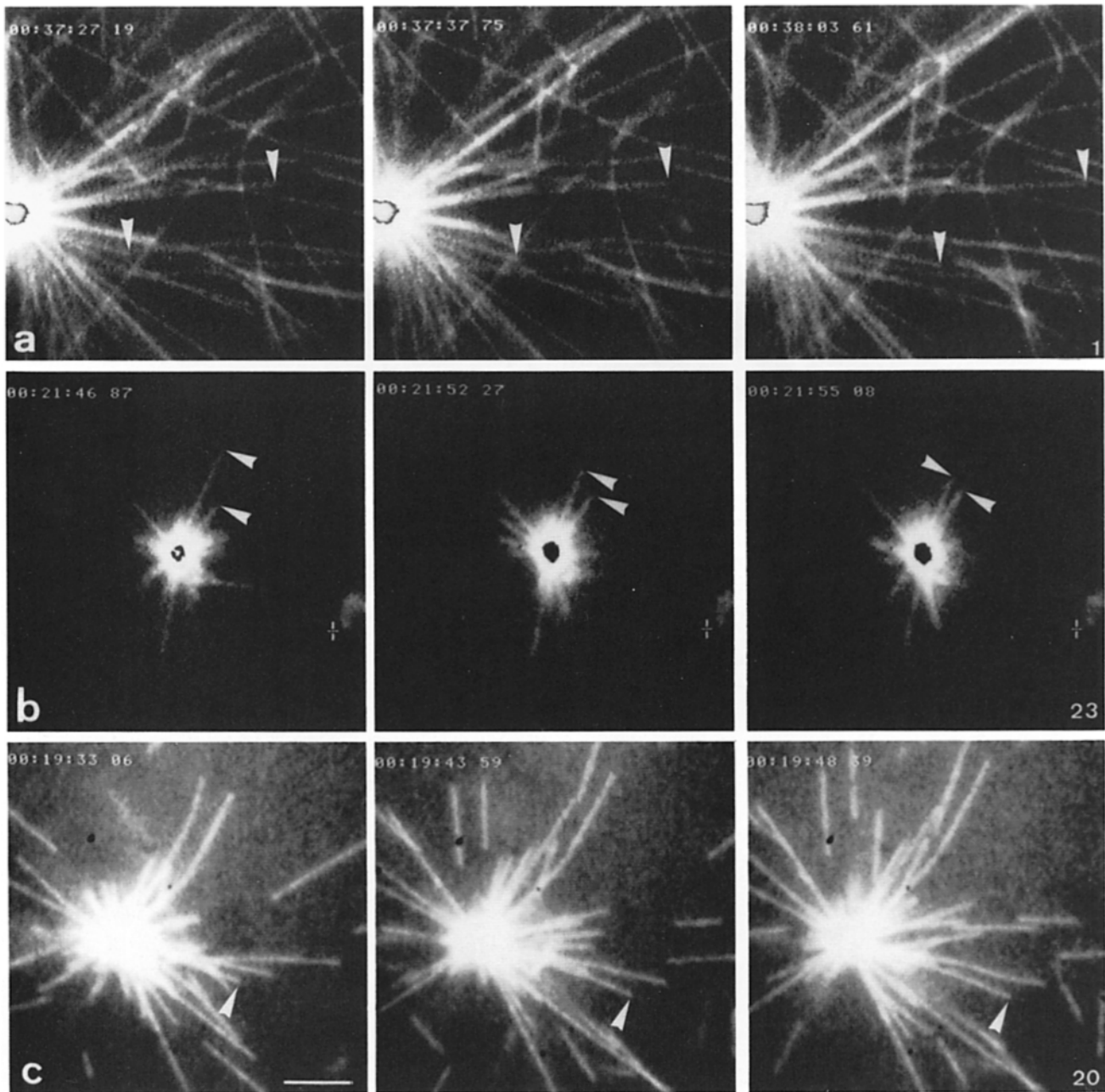


Figure 2. Effect of cyclin A- and cyclin B-dependent kinases on centrosome nucleated microtubules in egg extracts. An interphase extract was pre-incubated in the absence (a), or in the presence of 500 nM cyclin B (b) or 100 nM cyclin A (c) for 45 min. Centrosomes, rhodamine-labeled tubulin, and the anti-fade system were then added and the extract observed under the video microscope. The average histone kinase detected during the incubation with centrosomes is indicated in the lower right corner of each series of pictures. The arrow heads point to growing and shrinking microtubules. For each condition, we show three images separated by the time indicated in the upper left corner (h, min, s, 1/100). Bar, 5 μ m.

about the molecular mechanisms that determine them. The quantities used in the model are the probabilities $p_g(L, t)$ and $p_s(L, t)$ that a microtubule, in the growing (g) or shrinking (s) state has the length L at time t . The rates at which these probabilities change in time are shown schematically in Fig. 4. The dynamical equations for the time evolution are:

$$\frac{dp_g(L, t)}{dt} = \frac{V_g}{l} p_g(L - l, t) - (f_{cat} + \frac{V_g}{l}) p_g(L, t) + f_{res} p_s(L, t) \quad (1)$$

$$\frac{dp_s(L, t)}{dt} = \frac{V_s}{l} p_s(L + l, t) - (f_{res} + \frac{V_s}{l}) p_s(L, t) + f_{cat} p_g(L, t) \quad (2)$$

These equations have to be supplemented by the boundary conditions, whose form depends on the assumptions about nucleation processes at the centrosome. In general if one supposes a constant nucleation rate ν the evolution at the boundary is given by:

$$\frac{dp_g(0, t)}{dt} = \frac{-V_g}{l} p_g(0, t) + \nu p_s(0, t) \quad (3)$$

$$\frac{dp_s(0, t)}{dt} = \frac{V_s}{l} p_s(l, t) - \nu p_s(0, t) \quad (4)$$

These four equations can be solved (Grimmett and Stirzaker,

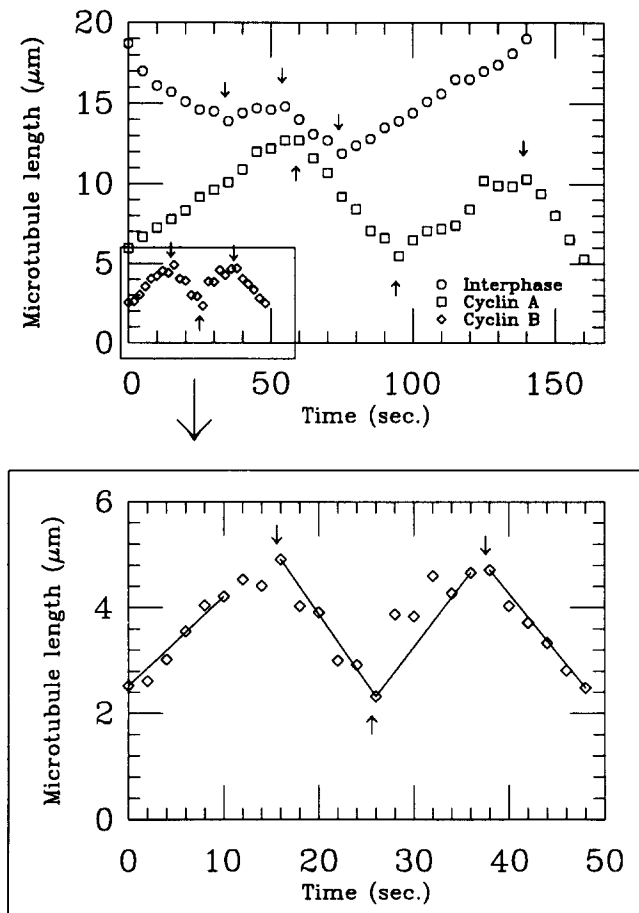


Figure 3. Changes in individual microtubule lengths were measured on images similar to those shown in Fig. 2 by displaying each image on the video screen as described in Materials and Methods (The bottom panel is an enlargement of the behavior of the cyclin B microtubule in top panel). Arrows indicate transitions between growing and shrinking phases. The straight lines in the lower panel illustrate the systematic method used to measure the velocities v_g and v_s . For the cyclin B extracts, time intervals of 10 s were used, while for the cyclin A extracts we used intervals of 15 s. Note that these values are then averaged over an ensemble of several dozen measurements, thus the exact choice of the procedure has no significant consequences on the results. The systematic errors in the measurements of the dynamical parameters from such curves are discussed in Materials and Methods.

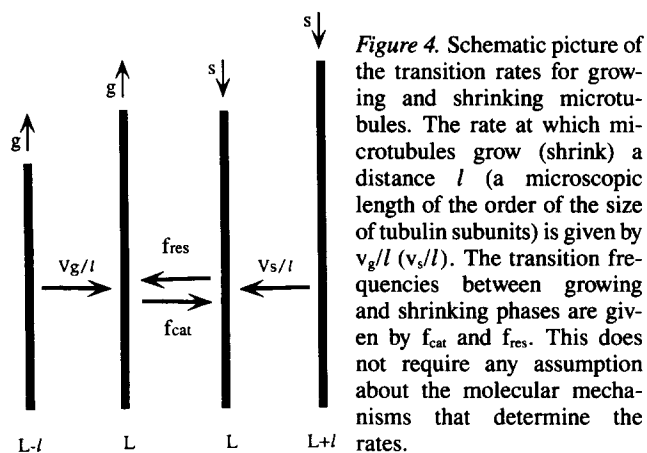


Figure 4. Schematic picture of the transition rates for growing and shrinking microtubules. The rate at which microtubules grow (shrink) a distance l (a microscopic length of the order of the size of tubulin subunits) is given by v_g/l (v_s/l). The transition frequencies between growing and shrinking phases are given by f_{cat} and f_{res} . This does not require any assumption about the molecular mechanisms that determine the rates.

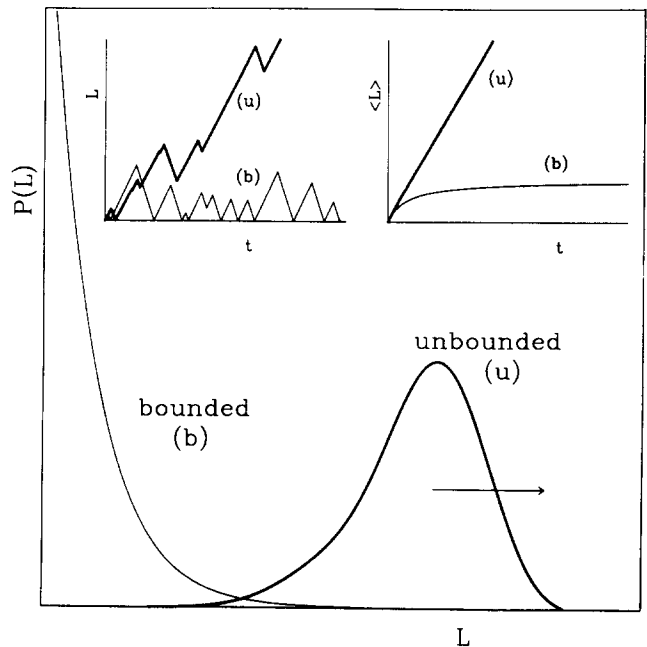


Figure 5. Time dependence of individual microtubule length (L , left inset), average length ($\langle L \rangle$, right inset) and length distribution ($P(L)$, main curves) according to a simple model of independent centrosome-nucleated, dynamic microtubules. The dynamic behavior of each microtubule is characterized by four stochastic parameters: f_{cat} , f_{res} , v_g , and v_s . For $f_{cat}v_s = f_{res}v_g$, a threshold is defined, corresponding to an average growth rate $J = 0$ (see equation 5). The average behavior of microtubules above and below this threshold is very different: above the threshold ($J > 0$), microtubules are in “unbounded” state (u); they can alternate between growing and shrinking phases (left inset) but, on average, they have a constant velocity of growth (right inset). $P(L)$ (main curve, right) propagates linearly in time (arrow), while its width increases with time like \sqrt{t} ; and its asymmetric shape evolves towards a Gaussian distribution. Below the threshold ($J < 0$), microtubules are in a “bounded” steady state (b); they alternate between growing and shrinking phases, but each microtubule, at some point, shrinks all the way back to the nucleating site (left inset). Because of constant re-nucleation, their average length $\langle L \rangle$ saturates at some constant value, given by equation 8 (right inset). $P(L)$ tends towards the steady state with a simple exponential distribution (main curve, left). It should be noted that a magnification of the curve in the right inset would show that the slope is initially bigger, because of proximity of the centrosome.

1982) with various initial conditions (we supposed all microtubules at the centrosome at $t = 0$). This allows to establish simple relationships between the parameters of microtubule dynamics, microtubule growth and their length distributions. The average velocity with which a given microtubule population grows, (J), is given by:

$$J = \frac{v_g f_{res} - v_s f_{cat}}{f_{cat} + f_{res}} \quad (5)$$

where v_g and v_s are average growth and shrinkage velocities for individual microtubules in their growing and shrinking phases. If we suppose that $v_g f_{res} > v_s f_{cat}$, so that J is positive, microtubules grow on average. In practice, microtubule growth would be limited only by the size of the container or by free tubulin subunits depletion. Although each microtubule can alternatively grow and shrink (Fig. 5, left inset, u),

the conditions are such that, on average, it keeps elongating with time (Fig. 5, right inset, *u*). We call this state of the microtubule assembly the unbounded state. For $v_g f_{res} < v_s f_{cat}$, on the other hand, J defined by equation 5 is negative, meaning that the ensemble of the microtubules does not grow on average; microtubules tend to disassemble all the way back to the centrosome (Fig. 5, left inset, *b*). Yet, at any time, a finite fraction of surviving microtubules is observed because of continuous re-nucleation at the centrosome (Fig. 5, left inset, *b*). This gives rise to a steady state, with a well-defined distribution of the microtubule lengths (Fig. 5, right inset, *b*) which we call the bounded state of microtubule assembly.

It should be noted that in this context, J represents the exact average growth only for microtubules that at no time shrink all the way back to the centrosome. In the presence of a nucleating centrosome the sign of its value determines always, however, whether a microtubule population reaches a steady state or grows on average.

We estimated J for centrosome nucleated microtubules in egg extracts by applying equation 5 to the values of the parameters measured in different conditions (Table I). The parameters of microtubule dynamics were supposed to be constant throughout each experiment. In interphase extracts, J is slightly positive (Table I) and thus microtubules should be in the unbounded state. This implies that the microtubules should not display a steady state length distribution and provides a theoretical interpretation of the results reported above: in interphase extracts, the growth of microtubules is limited by the size of the container and/or the depletion of the free tubulin subunit concentration. In extracts containing active cyclin dependent kinases, on the other hand, the estimated J values are all negative (Table I), predicting that, even in the presence of an unlimited supply of subunits, the initial growth of centrosome nucleated microtubules should saturate at some finite average length corresponding to the bounded state with its well-defined steady state length distribution.

We developed the model further in order to calculate the characteristics of microtubule length distributions in the unbounded and bounded states (Fig. 5, main diagram). In the unbounded state, the probability distribution given by $P(L, t) = p_g(L, t) + p_s(L, t)$ is not a steady state distribution; the microtubule length distribution should be strongly asymmetric early after the beginning of growth and then tend with time towards a Gaussian (which moves away from the centrosome with the average velocity J). It can be shown in perturbation theory that for long times it is of the form:

$$P(L, t) = \frac{1}{\sqrt{2\pi Dt}} \exp\left[-\frac{(L - Jt)^2}{2Dt}\right] \left[1 + C\left(\frac{(L - Jt)^3}{D^3 t^2} - \frac{3(L - Jt)}{D^2 t}\right) + \dots\right], \quad (6)$$

where the "effective diffusion constant," D , and the correction coefficient C are algebraic functions of the dynamical parameters, e.g., $D = 2f_{cat}f_{res}(v_g + v_s)^2/(f_{cat} + f_{res})^3$. In the bounded state, one can show that the steady state length distribution is exponential:

$$P(L) = \frac{1}{\langle L \rangle} e^{-L/\langle L \rangle}, \quad (L > 0) \quad (7)$$

with the average length L given by

$$\langle L \rangle = \frac{V_s V_g}{V_s f_{cat} - V_g f_{res}} \left(1 + l \frac{f_{cat}}{V_g}\right) \cong \frac{V_s V_g}{V_s f_{cat} - V_g f_{res}} \quad (8)$$

Here l is a microscopic length of the order of the size of tubulin subunits. Note that for any realistic values of the parameters we could neglect the term containing l . This last result had been already obtained in a similar context by T. Hill (Hill, 1987). It is important to stress that the mean length $\langle L \rangle$, given by Equation 8, does not depend on the nucleation rate ν , provided in this average we do not take into account the microtubules of zero length (empty nucleation sites). Thus the results of our measurements are not affected by possible changes in the nucleation properties of the centrosome due to the action of cyclins. The last column in Table I shows the values of $\langle L \rangle$ calculated with equation 8 for the dynamical parameters characterizing different extracts. One can clearly see that the cyclin B-dependent kinase should shorten the microtubules to a much larger extent than the cyclin A dependent kinase as expected from Figs. 1 and 2.

To compare quantitatively the length distributions of centrosome nucleated asters with the predictions of the theoretical model, we measured microtubule length distributions on the same video frames that were used to evaluate the parameters of microtubule dynamics reported in Table I. Unfortunately, it was impossible to measure all microtubules in these experiments. Those with ends close to the centrosome

Table II. Experimental and Theoretical Average Lengths of Visible Parts of Microtubules

		$\langle L \rangle_{\min}^{\max}$		L_{\min}	L_{\max}
		Experimental	Theoretical	(μm)	(μm)
		(μm)			
Interphase	Long + free polymer				
Cyclin A					
25 nM	Long				
50 nM	8.3 \pm 0.2 (n = 136)	8.8 \pm 0.4	5	20	
100 nM	8.4 \pm 0.2 (n = 325)	8.8 \pm 0.5	5	20	
	8.0 \pm 0.1 (n = 461)	8.4 \pm 0.5	5	20	
	9.4 \pm 0.3 (n = 303)	9.0 \pm 0.4	5	20	
Cyclin B					
500 nM	5.2 \pm 0.1 (n = 396)	4.9 \pm 0.4	3	20	
	4.1 \pm 0.1 (n = 135)	4.8 \pm 0.4	3	20	

The values represent average lengths for microtubules longer than L_{\min} and shorter than L_{\max} . L_{\min} is larger for cyclin A- than cyclin B-treated extracts, because centrosomes nucleate more microtubules in this case, making difficult measurements close to the centrosome. The value of L_{\max} is imposed by the video setup. Microtubule lengths were estimated in every fifth video frame and the given value is the average with its expected error (n indicates the total number of microtubules analyzed in each experiment). The theoretical values shown were calculated using the dynamical parameters from Table I. The calculated exponential distribution (equations 7 and 8) was corrected to take into account the geometry of the experimental setup (see Materials and Methods and Fig. 6, inset). The errors rise from the uncertainties for the values of $\langle L \rangle$. (Note that uncertainties for the average lengths presented here are much smaller than the errors for $\langle L \rangle$ presented in Table I. This statistical effect is due to the averaging within the finite window (L_{\min} , L_{\max})).

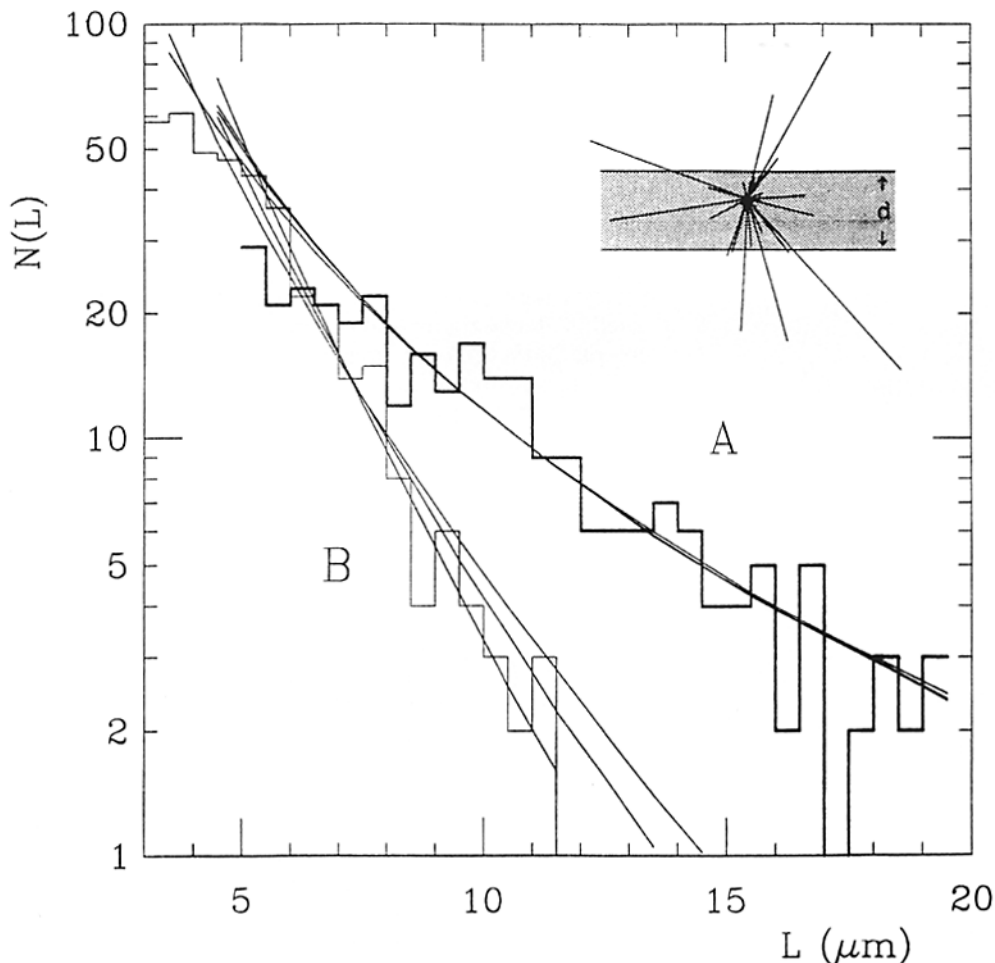


Figure 6. Experimental and theoretical length distributions of centrosome nucleated microtubules in cyclin A- (*A*) and cyclin B- (*B*) treated extracts. The length measurements were performed on every fifth video frame of the recordings (same data as those used to estimate the dynamical parameters shown in Table I). The total number of microtubules measured were 336 (cyclin A) and 303 (cyclin B). Only microtubules with lengths larger than $L_{\min} = 5 \mu\text{m}$ (cyclin A) or $3 \mu\text{m}$ (cyclin B) and smaller than $L_{\max} = 20 \mu\text{m}$ were considered. The theoretical curves were obtained assuming an exponential length distribution (equation 7), $\langle L \rangle$ being calculated using the values of the dynamical parameters shown in Table I. It should be noted that in the experiment we can only measure the two-dimensional projection onto the focal plane (see inset) in a window between 5 (3, for cyclin B) and 20 microns. To compare the theoretical values with the experiments we corrected the former for the geometry of the experimental setup (see Materials and Methods). This cor-

rection is important but not very sensitive to the exact value of depth of field (d), nor to the exact position of the centrosome within the area. The three curves obtained for microtubules in cyclin A treated extracts were calculated for $d = 1 \mu\text{m}$ and $2 \mu\text{m}$ and the extreme positions of the centrosome. Similar curves were calculated in the case of cyclin B (not shown). The three calculated curves shown for microtubules in cyclin B-treated extracts have been obtained taking into account the uncertainties on the dynamical parameters (see Table I). Similar curves were calculated for cyclin A (not shown). The agreement between the experimental data (histograms) and the theoretical curves (continuous lines) obtained using Equation 7 does not involve any fitting parameters.

were not visible and those larger than the optical field could not be measured either (Fig. 2). Therefore we systematically measured only microtubules with a length exceeding some lower cut-off value L_{\min} (the size of the blurred centrosomal area) and smaller than the size of the optical field L_{\max} (see Materials and Methods). The other difficulty was that we were measuring microtubules, that were growing in three dimensions, on a two-dimensional screen. Therefore, we corrected the calculated theoretical lengths for these two geometrical effects before comparing them with experimental values (see Materials and Methods). The corrected theoretical lengths calculated from the dynamical parameters using equations 7 and 8 and the measured lengths are shown in Table II. The theoretical and experimental values agree within the estimated error limits (note that the errors for theoretical values correspond to the errors in the measured values of the dynamical parameters, reported in Table I, which were used to calculate the average lengths). Therefore, equation 8 seems to provide a good approximation for the average length of the bounded state appearing when $J < 0$.

To check whether the form of the length distribution in the bounded state also agreed with equation 7, we measured the whole distributions for one experiment carried out with cyclin A and the other with cyclin B, for which we had established the dynamical parameters (Table I). Fig. 6 shows, in addition to the measured distributions, the theoretical curves, in which again we took into account the geometrical effects connected with the microscopy. The agreement between the calculated and measured distributions is striking. In fact, it may seem so good that a word of caution is needed. Assembly of centrosome nucleated microtubules is a complex collective phenomenon and one might expect microtubule dynamics to be influenced by the flexibility of polymers, the detailed geometry of the growth which may introduce perturbations in the spatial distribution of diffusing subunits, and, as a consequence, effective interactions between growing polymers. Also v_g and v_s may not be perfectly constant in the extract (cf., Fig. 3). The present model did not take into account all these phenomena. The reason why it seems to describe so adequately the dynamic structure of the asters is probably due to the fact that the values of the dynamical

parameters are spatially averaged. Also, the measurements were not performed in the vicinity of the centrosome where concentration in free monomer should be most affected by growing polymer. It is important to stress, however, that the agreement between the experimental and theoretical curves, for both cyclin A- and cyclin B-treated extracts, is not due to any fitting procedure. In fact, there are no adjustable parameters neither in the model nor in the geometrical corrections made to compare the curves.

Discussion

Modulation of the Function of p34^{cdc2} by Different Cyclins

In this study, we used heterologous cyclin A and cyclin B (of human and sea urchin origin, respectively), produced in bacteria, to activate cdc2 kinase in the extracts. Therefore one must remain cautious about the possible implications of our present results for the *in vivo* physiological situation. It seems quite clear that the cyclin B used here and previously by (Belmont et al., 1990) does what the homologous enzyme does *in vivo*. First, it has exactly the same effect as the cdc2 kinase purified from starfish (Verde et al., 1990), second it produces very short asters which look very much like those observed in mitotic cells during metaphase when the cyclin B-dependent kinase is mostly active. It is likely that what we observe with the cyclin A, namely no effect on f_{cat} and a slight effect on f_{res} , elimination of spontaneous assembly but little shortening of microtubules, is physiological. Indeed, *in vivo*, microtubules remain long during prophase when this kinase is already activated (Karsenti, 1991; Merdes et al., 1991). It remains however that complete generalization of the specific effect of cyclin A- and cyclin B-dependent kinases on microtubule dynamics will require more experiments carried out with homologous and other cyclins both *in vivo* and *in vitro*. In any case, the present experiments clearly demonstrate that the functional specificity of the catalytic subunit p34^{cdc2} can be altered by the nature of the cyclin to which it is associated. Indeed, when cyclin A is added to an extract at the concentration of 1 μ M, 90% of the p34^{cdc2} present in the extract becomes associated with cyclin A. Moreover, at least 80% of the kinase activity measured on histone H1 can be attributed to this kinase and not to the other cdc2 like molecule that binds to cyclin A in these extracts, namely p33^{cdk2} (Clarke et al., 1992). Since under such conditions, f_{cat} is not increased and microtubules do not shrink, we conclude that this cyclin A cdc2 kinase complex does not see the molecule present in the extract that induces microtubule shrinkage when phosphorylated by the cyclin B cdc2 complex. Cyclin A has also been shown not to affect endosome fusion in the same egg extracts (Thomas et al., 1992). In a different system, cyclin A does not activate the degradation machinery responsible for abrupt cyclin proteolysis during metaphase whereas cyclin B does (Luca et al., 1991). By contrast, the cyclin A- dependent kinase seems to be a better enzyme than the cyclin B-dependent kinase to phosphorylate centrosomes and increase their microtubule nucleating activity (Buendia et al., 1992). Therefore, there is growing evidence indicating that the cyclin A-dependent kinase has distinct functions from the cyclin B-dependent kinase. The known differences suggest that in addition

to its function at the G1-S transition (Pagano et al., 1992), the cyclin A-dependent kinase fulfills specific functions in prophase and that there is not a complete overlap of functions between cyclin A and cyclin B (Buendia et al., 1991).

Biochemical Regulation of Microtubule Dynamics

The molecular mechanism through which cdc2 kinases affect specifically microtubule dynamics are not yet elucidated. A plausible hypothesis is that microtubule associated proteins (MAPs) are phosphorylated and partially inactivated by the cyclin-dependent kinases. The situation seems complex however. First, both cyclin A- and cyclin B-dependent kinases do not reduce v_g . Given the high value observed for this parameter (10 μ m/min) in the extracts compared to values observed for pure tubulin at similar concentrations (1–2 μ m/min), there must be MAPs that increase the on rate of tubulin subunits at microtubule ends. X-MAP could be such a MAP (Gard and Kirschner, 1987b). If this were the case, however, this MAP should not be inactivated by either cyclin A- or cyclin B-dependent kinases since v_g is not reduced but rather increased in extracts treated by these kinases. f_{res} seems to be slightly reduced both by cyclin A and cyclin B. The reason for this is obscure but this may suggest that different MAPs could regulate v_g and f_{res} . Finally, f_{cat} is specifically increased by cyclin B. This strongly suggests that a specific factor is involved in regulating this parameter and that its activity is increased by a cyclin B-dependent kinase phosphorylation event. Whether this effect is direct or involves a cascade of kinases (Gotoh et al., 1991) remains to be determined. The multiplicity of factors involved in the regulation of the different parameters of microtubule dynamics begins only to be approached at the biochemical level (Simon et al., 1992). A microtubule severing factor activated by cyclin B has been recently reported to be present in egg extracts (Vale, 1991). We have tested its possible involvement in increasing f_{cat} by adding fluorescently labeled taxol stabilized microtubules to an interphase extract in the absence or presence of cyclin A and cyclin B. In the interphase extract microtubules remained stable whereas both in the cyclin A- and cyclin B-treated extracts, microtubules became severed with exactly the same kinetics (<3 min, not shown). Therefore, the increase in f_{cat} observed in cyclin B-treated extracts cannot be due to an activation of the severing factor. A specific molecular mechanism by which f_{cat} is regulated remains to be discovered.

From Interphase to Mitosis

It is now clear that the reorganization of microtubules which ultimately leads to mitotic spindle assembly involves a complex regulatory network and that cyclin-dependent kinases may have specific functions at different times in prophase and during metaphase. It has been previously proposed that microtubules become more dynamic during mitosis solely because the free tubulin concentration decreases in the finite volume of the cell as a result of increased polymer mass produced by the higher nucleating capacity of centrosomes (Kirschner and Mitchison, 1986, 1987). Although this may be part of the process, the regulation of the microtubule nucleating activity of centrosomes, of a microtubule severing system and of f_{cat} and f_{res} seem to be independently regulated by cyclin A- and cyclin B-dependent kinases. A general

scheme of how microtubules are reorganized between S-phase and metaphase is beginning to emerge. When DNA replication is completed, in early prophase, the cyclin A which was essentially nuclear (Pines and Hunter, 1991), becomes partially cytoplasmic and associated with the centrosomes (Pagano et al., 1992). According to previous in vitro results this kinase could phosphorylate centrosomes and increase their nucleating activity (Buendia et al., 1992). Indeed, at this time, the nucleating activity of centrosomes seems to increase in many cases (Bré et al., 1990; Merdes et al., 1991). In the same time, the same kinase severs interphasic microtubules leading to progressive disappearance of the interphasic network and the centrosomal microtubules would reach a steady state distribution because f_{res} is decreased. However, microtubules remain long on average because f_{cat} is not increased (Merdes et al., 1991). This specific behavior of microtubules in prophase is probably required to position properly the centrosomes in the cell through dynamic interactions with the cell cortex, which, in turn, may determine the orientation of the spindle axis (Hyman and White, 1987). When prophase is completed, the kinase activity associated with cyclin B rises, activating the factor that increases f_{cat} and microtubules shrink. Preferential orientation of microtubules towards mitotic chromosomes and spindle assembly would result from a local decrease in f_{cat} around the chromosomes, leading to longer and more long lived microtubules in this area (Karsenti et al., 1984; Sawin and Mitchison, 1991).

The Predictions of the Mathematical Model

The mathematical model presented here relates microtubule length with the four parameters of dynamic instability, without making any assumption concerning the molecular mechanisms underlying dynamic instability. Even though the experimental results used to test this theoretical relation are subject to important statistical limitations, the adequation between the length predicted by the equations from the dynamical parameters and the actual lengths measured is so good that we must conclude that the equations represent fairly well the behavior of microtubules. In particular we showed that the stochastic behavior of microtubules can result in the production of well defined steady state length distributions. The steady-state length distributions of centrosome-nucleated microtubules observed in an infinite volume containing an unlimited supply of subunits seem indeed to be determined by the relative values of the dynamical parameters.

The experimental results reported in this paper have demonstrated that extensive microtubule shortening in the bounded state is correlated rather with an increase in f_{cat} than with a decrease in f_{res} . Indeed, equation 8 predicts that changing f_{cat} and f_{res} should have different effects on the average steady state length of microtubules. According to this formula, $\langle L \rangle$ can decrease all the way to zero when f_{cat} is increased. This is not the case if one reduces $\langle L \rangle$ by decreasing f_{res} : even at $f_{res} = 0$, the average length is finite and equal to v_g/f_{cat} . In interphase extracts, for example, if one equals f_{res} to zero, v_g/f_{cat} gives a value of 10–15 μm for $\langle L \rangle$. Therefore, if microtubules behave as predicted by this model, and they seem to do so to a large extent, increasing f_{cat} is the most efficient way of shortening the steady state average length of microtubule asters. This is what cyclin B

indeed does: it shrinks microtubules mainly by increasing strongly f_{cat} .

The effect of cyclin A-dependent kinase is much more subtle: this kinase seems to modify only slightly the dynamical parameters of the microtubules. Such small modifications, however, are sufficient to change significantly the state of the asters: the long, interphase-like microtubules which constantly tend to grow, are changed to long but fully dynamic asters with specific steady state lengths. This subtle effect can be clearly understood within the framework of the theoretical model. Equation 5 shows that when $v_g f_{res} = v_s f_{cat}$, the average growth rate $J = 0$ and $\langle L \rangle$ tends towards infinity. This represents a singularity, or a threshold, at the boundary between infinite microtubule growth and the establishment of steady state dynamics. The presence of such a threshold makes it possible to change completely the microtubule length distribution by varying only a little the dynamical parameters. In fact, in egg extracts (and probably in vivo), the microtubule system seems to operate close to the threshold defined by $J = 0$. This is probably why minor changes in the dynamical parameters are sufficient to induce important alterations in microtubule lengths and aster organization: the interphase and cyclin-treated extracts simply lie on different sides of the threshold. This idea, introduced and quantitatively verified here with the help of a simple theoretical model, shows on a precise example how the molecules connected with the regulation of the cell cycle can modify cellular structures by local and sometimes rather subtle changes of the dynamical properties of assembling-disassembling processes.

We would like to thank A. C. Maggs, G. Mantica, R. McIntosh, T. Mitchison, and T. Salmon for valuable discussions and help, M. Pagano for providing us with cyclin A, and M. Glotzer for giving us cyclin B. S. Leiber would like to thank particularly M. F. Carlier and D. Pantaloni for many discussions and constant encouragements.

This work was partially supported by a short term EMBO fellowship to M. Dogterom and a Human Frontier Science Program grant to E. Karsenti.

Received for publication 5 May 1992.

References

- Belmont, L. D., A. A. Hyman, K. E. Sawin, and T. J. Mitchison. 1990. Real-time visualization of cell cycle-dependent changes in microtubule dynamics in cytoplasmic extracts. *Cell*. 62:579–589.
- Blow, J. J., and R. A. Laskey. 1986. Initiation of DNA replication in nuclei and purified DNA by a cell-free extract of *Xenopus* eggs. *Cell*. 47:577–587.
- Bornens, M., M. Paintrand, J. Berges, M. C. Marty, and E. Karsenti. 1987. Structural and chemical characterization of isolated centrosomes. *Cell Motil. Cytoskeleton*. 8:238–249.
- Bré, M. H., R. Pepperkok, A. M. Hill, N. Levilliers, W. Ansorgue, E. H. K. Stelzer, and E. Karsenti. 1990. Regulation of microtubule dynamics and nucleation during polarization in MDCK II cells. *J. Cell Biol.* 111:3013–3021.
- Buendia, B., P. R. Clarke, M. A. Félix, E. Karsenti, D. Leiss, and F. Verde. 1991. Regulation of protein kinases associated with cyclin A and cyclin B and their effect on microtubule dynamics and nucleation in *Xenopus* egg extracts. *C.S.H. Quant. Symp. Biol.* 56:523–532.
- Buendia, B., G. Draetta, and E. Karsenti. 1992. Regulation of the microtubule nucleating activity of centrosomes in *Xenopus* egg extracts: role of cyclin A associated kinase. *J. Cell Biol.* 116:1431–1442.
- Carlier, M. F. 1991. Nucleotide hydrolysis in cytoskeletal assembly. *Curr. Opin. Cell Biol.* 3:12–17.
- Cassimeris, L., N. K. Pryer, and E. D. Salmon. 1988. Real time observations of microtubule dynamic instability in living cells. *J. Cell Biol.* 107:2223–2231.
- Clarke, P., D. Leiss, M. Pagano, and E. Karsenti. 1992. Cyclin A- and cyclin B-dependent kinases are regulated by different mechanisms in *Xenopus* egg extracts. *EMBO (Eur. Mol. Biol. Organ.) J.* 11:1751–1761.
- Dabauvalle, M. C., K. Loos, H. Merkert, and U. Scheer. 1991. Spontaneous

- assembly of pore complex-containing membranes ("annulate lamellae") in *Xenopus* egg extract in the absence of chromatin. *J. Cell Biol.* 112:1073-82.
- Draetta, G., and D. Beach. 1989. The mammalian cdc2 protein kinase: mechanism of regulation during the cell cycle. *J. Cell Sci. Suppl.* 12:21-27.
- Evans, L., T. S. Mitchison, and M. W. Kirschner. 1985. Influence of the centrosome on the structure of nucleated microtubules. *J. Cell Biol.* 100:1185-1191.
- Félix, M.-A., J. Pines, T. Hunt, and E. Karsenti. 1989. A post-ribosomal supernatant from activated *Xenopus* eggs that displays post-translationally regulated oscillation of its cdc2+ mitotic kinase activity. *EMBO (Eur. Mol. Biol. Organ.) J.* 8:3059-3069.
- Félix, M. A., P. Cohen, and E. Karsenti. 1990. Cdc2 H1 kinase is negatively regulated by a type 2A phosphatase in the *Xenopus* early embryonic cell cycle: evidence from the effects of okadaic acid. *EMBO (Eur. Mol. Biol. Organ.) J.* 9:675-683.
- Gard, D., and M. Kirschner. 1987b. A microtubule-associated protein from *Xenopus* eggs that specifically promotes assembly at the plus end. *J. Cell Biol.* 105:2203-2215.
- Gildersleeve, R. F., A. R. Cross, K. E. Cullen, A. P. Fagen, and R. C. Williams, Jr. 1992. Microtubules grow and shorten at intrinsically variable rates. *J. Biol. Chem.* 267:7995-8006.
- Giordano, A., P. Whyte, E. Harlow, B. R. Franza, D. Beach, and G. Draetta. 1989. A 60 kD cdc2-associated polypeptide complexes with the E1A proteins in Adenovirus-infected cells. *Cell.* 58:981-990.
- Glotzer, M., A. W. Murray, and M. W. Kirschner. 1991. Cyclin is degraded by the ubiquitin pathway. *Nature (Lond.)*. 349:132-138.
- Gotoh, Y., E. Nishida, S. Matsuda, N. Shiina, H. Kosako, K. Shiokawa, T. Akiyama, K. Ohta, and H. Sakai. 1991. In vitro effects on microtubule dynamics of purified *Xenopus* M phase-activated MAP kinase. *Nature (Lond.)*. 349:251-254.
- Grimmett, G. R., and D. R. Storzaker. 1982. Probability and random processes. Clarendon Press, Oxford.
- Haferkorn, H. 1981. Optik. V. H. Deutsch, editor. Thun, Frankfurt/M. 512-514.
- Heald, R., and F. McKeon. 1990. Mutations of phosphorylation sites in lamin A that prevent nuclear lamina disassembly in mitosis. *Cell.* 61:579-589.
- Hill, T. L. 1987. Linear Aggregation Theory in Cell Biology. Springer Verlag.
- Hunt, T. 1989. Maturation promoting factor, cyclin and the control of M-phase. *Curr. Op. Cell Biol.* 1:286-274.
- Hunter, T., and J. Pines. 1991. Cyclins and cancer. *Cell.* 66:1071-1074.
- Hutchison, C. J., D. Brill, R. Cox, J. Gilbert, I. Kill, and C. C. Ford. 1989. DNA replication and cell cycle control in *Xenopus* egg extracts. *J. Cell Sci. Suppl.* 12:197-212.
- Hyman, A., D. Drechsel, D. Kellogg, S. Salser, K. Sawin, P. Steffen, L. Wordeman, and T. Mitchison. 1991. Preparation of modified tubulins. *Methods Enzymol.* 196:478-485.
- Hyman, A. A., and J. G. White. 1987. Determination of cell division axes in the early embryogenesis of *Caenorhabditis elegans*. *J. Cell Biol.* 105:2123-2135.
- Karsenti, E. 1991. Mitotic spindle morphogenesis in animal cells. *Semin. Cell Biol.* 2:251-260.
- Karsenti, E., J. Newport, R. Hubble, and M. Kirschner. 1984. Interconversion of metaphase and interphase microtubule arrays, as studied by the injection of centrosomes and nuclei into *Xenopus* eggs. *J. Cell Biol.* 98:1730-1745.
- Karsenti, E., F. Verde, and M. A. Félix. 1991. Role of type 1 and type 2A protein phosphatases in the cell cycle. *Adv. Prot. Phosph.* 6:453-482.
- Kirschner, M., and T. Mitchison. 1986. Beyond self-assembly: from microtubules to morphogenesis. *Cell.* 45:329-342.
- Kobayashi, H., J. Minshull, C. Ford, R. Golsteyn, R. Poon, and T. Hunt. 1991. On the synthesis and destruction of A- and B-type cyclins during oogenesis and meiotic maturation in *Xenopus laevis*. *J. Cell Biol.* 114:755-765.
- Lohka, M., and J. Maller. 1985. Induction of nuclear envelope breakdown, chromosome condensation, and spindle formation in cell-free extracts. *J. Cell Biol.* 101:518-523.
- Lohka, M. J., and J. L. Maller. 1988. Induction of metaphase chromosome condensation in human sperm by *Xenopus* egg extracts. *Exp. Cell Res.* 179:303-309.
- Luca, F. C., E. K. Shibuya, C. E. Dohrmann, and J. V. Ruderman. 1991. Both cyclin AΔ60 and BΔ97 are stable and arrest cells in M-phase, but only cyclin BΔ97 turns on cyclin destruction. *EMBO (Eur. Mol. Biol. Organ.) J.* 10:4311-4320.
- McIntosh, J. R., and G. E. Hering. 1991. Spindle fiber action and chromosome movement. *Int. Rev. Cell Biol.* 7:403-426.
- Merdes, A., E. H. K. Stelzer, and J. De Mey. 1991. The three-dimensional architecture of the mitotic spindle, analyzed by confocal fluorescence and electron microscopy. *J. Elect. Microsc. Tech.* 18:61-73.
- Minshull, J. 1989. Cyclin and MPF: driving mitosis. *BioEssays* 11:149-151.
- Minshull, J., R. Golsteyn, C. S. Hill, and T. Hunt. 1990. The A- and B-type cyclin associated cdc2 kinases in *Xenopus* turn on and off at different times in the cell cycle. *EMBO (Eur. Mol. Biol. Organ.) J.* 9:2865-75.
- Mitchison, T., and M. Kirschner. 1984a. Dynamic instability of microtubule growth. *Nature (Lond.)*. 312:237-242.
- Mitchison, T., and M. Kirschner. 1984b. Microtubule assembly nucleated by isolated centrosomes. *Nature (Lond.)*. 312:232-237.
- Mitchison, T. J., and M. Kirschner. 1987. Some thoughts on the partitioning of tubulin between monomer and polymer under conditions of dynamic instability. *Cell Biophys.* 11:35-55.
- Mitchison, T. J., and K. E. Sawin. 1990. Tubulin flux in the mitotic spindle: where does it come from, where is it going? *Cell Motil. Cytoskeleton.* 16:93-98.
- Murray, A. W., and M. W. Kirschner. 1989. Cyclin synthesis drives the early embryonic cell cycle. *Nature (Lond.)*. 339:275-280.
- Newport, J. 1987. Nuclear reconstitution in vitro: Stages of assembly around protein-free DNA. *Cell.* 48:205-217.
- Newport, J., and T. Spann. 1987. Disassembly of the nucleus in mitotic extracts: membrane vesicularization, lamin disassembly, and chromosome condensation are independent processes. *Cell.* 48:219-230.
- Nurse, P. 1990. Universal control mechanism regulating onset of M-phase. *Nature (Lond.)*. 344:503-508.
- Pagano, M., R. Pepperkok, F. Verde, W. Ansorgue, and G. Draetta. 1992. Cyclin A is required at two points in the human cell cycle. *EMBO (Eur. Mol. Biol. Organ.) J.* 11:961-971.
- Particle Data Group. 1990. Review of particle properties. *Phys. Lett. B.* 239:28-38.
- Peter, M., J. Nakagawa, M. Dorée, J. C. Labbé, and E. A. Nigg. 1990. In vitro disassembly of the nuclear lamina and M phase-specific phosphorylation of lamins by cdc2 kinase. *Cell.* 61:591-602.
- Pines, J., and T. Hunter. 1990. Human cyclin A is adenovirus E1A-associated protein p60 and behaves differently from cyclin B. *Nature (Lond.)*. 346:760-763.
- Pines, J., and T. Hunter. 1991. Human cyclins A and B1 are differentially located in the cell and undergo cell cycle-dependent nuclear transport. *J. Cell Biol.* 115:1-17.
- Salmon, E. D. 1989. Microtubule dynamics and chromosome movement. J. S. Hyams, and B. R. Brinkley, editors. Academic Press, London. 119-181.
- Sawin, K. E., and T. J. Mitchison. 1991. Mitotic spindle assembly by two different pathways in vitro. *J. Cell Biol.* 112:925-940.
- Schulze, E., and M. Kirschner. 1988. New features of microtubule behaviour. *Nature (Lond.)*. 334:356-359.
- Simon, J. R., S. F. Parsons, and E. D. Salmon. 1992. Buffer conditions and non-tubulin factors critically affect the microtubule dynamic instability of sea urchin egg tubulin. *Cell Motil. Cytoskeleton.* 21:1-14.
- Thomas, L., P. R. Clarke, M. Pagano, and J. Gruenberg. 1992. Inhibition of membrane fusion in vitro via cyclin B but not cyclin A. *J. Biol. Chem.* 267:6183-6187.
- Tuomikoski, T., M.-A. Félix, M. Dorée, and J. Gruenberg. 1989. Inhibition of endocytic vesicle fusion in vitro by the cell-cycle control protein kinase cdc2. *Nature (Lond.)*. 342:942-945.
- Vale, R. D. 1991. Severing of stable microtubules by a mitotically activated protein in *Xenopus* egg extracts. *Cell.* 64:827-839.
- Verde, F., J. C. Labbé, M. Dorée, and E. Karsenti. 1990. Regulation of microtubule dynamics by cdc2 protein kinase in cell-free extracts of *Xenopus* eggs. *Nature (Lond.)*. 343:233-238.
- Walker, R. A., E. T. O'Brien, N. K. Pryer, M. F. Sobeiro, W. A. Voter, H. P. Erickson, and E. D. Salmon. 1988. Dynamic instability of individual microtubules analyzed by video light microscopy: rate constants and transition frequencies. *J. Cell Biol.* 107:1437-1448.
- Ward, G. E., and M. W. Kirschner. 1990. Identification of cell cycle-regulated phosphorylation sites on nuclear lamin C. *Cell.* 61:561-577.